Received April 2000
Accepted August 2000

On volumetric locking of low-order solid and solid-shell elements for finite elastoviscoplastic deformations and selective reduced integration

Stefan Doll, Karl Schweizerhof, Ralf Hauptmann and Christof Freischläger
Institut für Mechanik, Universität Karlsruhe, Germany

Keywords *Finite elements, Shells, Elastic-viscoplastic model, Deformation, Integration*

Abstract *As known from nearly incompressible elasticity, selective reduced integration (SRI) is a simple and effective method of overcoming the volumetric locking problem in 2D and 3D solid elements. This method of finite elastoviscoplasticity is discussed as are its well-known limitations. In this context, an isochoric-volumetric decoupled material behavior is assumed and thus the additive deviatoric-volumetric decoupling of the consistent algorithmic moduli tensor is essential. By means of several numerical examples, the performance of elements using selective reduced integration is demonstrated and compared to the performance of other elements such as the enhanced assumed strain elements. It is shown that a minor modification, with little numerical effort, leads to rather robust element behaviour. The application of this process to so-called solid-shell elements for thin-walled structures is also discussed.*

1. Introduction

It is a well-known fact, that the three-dimensional standard linear eight-node displacement element (here denoted as Q1) exhibits severe locking for nearly or fully incompressible material. Rubber elasticity or metal plasticity are examples for nearly incompressible material behavior. Rubber is characterized by a large ratio of the bulk modulus to the shear modulus. In metal plasticity the plastic deformation is isochoric, i.e. fully incompressible, and the compressible part is a result from elastic deformations only, which remain small in many applications. In both cases reliable results with the standard Q1 element cannot be expected. Due to the volumetric locking behavior of the Q1 element, additional measures are necessary to overcome this problem. Various methods are known from literature and are currently discussed. Among others, a brief review of some of these methods is given in the following as a reference for the developments shown in this contribution. Our focus is particularly on the capabilities concerning finite non-linear deformations:

Engineering Computations,
Vol. 17 No. 7, 2000, pp. 874-902.

(1) The Q1/P0 element proposed by Simo *et al.* (1985) is based on a three-field hybrid formulation with independent constant pressure and constant dilatation. Both, the pressure and the dilatation variables, are eliminated by static condensation. It is well known that this element does not pass the LBB condition. Thus as shown in Simo (1992) the use of the Q1/P0 element is hampered by hour-glassing under certain loading conditions.

(2) The non-linear versions of the enhanced assumed strain (EAS) element based on suggestions by Simo (1992) and Simo *et al.* (1993) have been a considerable improvement concerning bending dominated problems. Also volumetric locking can be avoided by the appropriate choice of parameters. However, a severe drawback of this formulation concerning efficiency is the static condensation procedure of the internal degrees of freedom needed at element level in every iteration of the global Newton-Raphson solution scheme. Also additional storage is required for the internal degrees of freedom. A second problem is, as noted by Wriggers and Reese (1996), the occurrence of instabilities under certain loading states in the larger deformation case. Further developments on this method with some improvements concerning the mentioned drawbacks are, for example, reported by Nagtegaal and Fox (1996), Korelc and Wriggers (1996) and Glaser and Armero (1997). However, no general stable method is available yet. Associated with the enhancement of the strains an artificial material model dependency on the kinematic relations is introduced. Thus stability investigations, in particular in the large deformation regime have to take into account the material status and behavior at a certain state.

(3) In the so-called $\bar{\boldsymbol{F}}$ method the standard deformation gradient $\boldsymbol{F}$ is replaced by a modified deformation gradient $\bar{\boldsymbol{F}} = (\bar{J}/J)^{1/3}\boldsymbol{F}$ with $J = \det \boldsymbol{F}$ and $\bar{J} = constant$. The dilatation $\det \bar{\boldsymbol{F}} = \bar{J}$ is constant within the element and is not treated as an independent variable. The mean dilatation approach, originally suggested by Nagtegaal *et al.* (1974), leads with $\bar{J} = \int_V J dV / \int_V dV$ to the $\bar{\boldsymbol{F}}_{\text{Nag}}$ element. This element recovers the Q1/P0 element identically. Using the dilatation $\bar{J} = J_0 = \det \boldsymbol{F}_0$ at the element center results in the $\bar{\boldsymbol{F}}_{\text{Mor}}$ element by Moran *et al.* (1990) (see also de Souza Neto *et al.* (1996) for a slightly different element). The $\bar{\boldsymbol{F}}$ elements also show artificial instabilities in some situations (see also section 7.3.2) under certain loading conditions in the large strain regime.

(4) The selective reduced integration method is applicable consistently only for material models with independent isochoric and volumetric behavior. Full numerical integration is employed for the isochoric terms while selective reduced integration is employed for the volumetric terms of the internal force vector and the tangent stiffness matrix (Liu *et al.*, 1992; 1994) for the treatment of pure elasticity at finite strains). In Hughes (1987) the SRI is discussed for linear elasticity and some historical remarks are given.

The main well-known advantages of the SRI method are its simplicity and the little additional computational effort compared to the standard displacement element. The standard structure of the internal force vector and the stiffness matrix can be used without modifications. Only additional integration points have to be introduced. This additional effort is relatively small, e.g. one additional integration point at the center of a Q1 element. Using the Q1/P0, EAS or $\bar{\boldsymbol{F}}$ elements instead of the SRI element, the modifications of the internal force vector or the stiffness matrix can be much more time consuming. We refer to Fried (1974), Malkus (1976), Hughes (1977; 1980; 1987) and Malkus and Hughes (1978) for a detailed investigation of the SRI method and its equivalence with certain mixed finite element methods. These investigations do not include the case of finite deformation elasto-viscoplasticity as presented in this contribution.

However, one advantage of the Q1/P0, EAS or $\bar{\boldsymbol{F}}$ elements over the SRI element has to be kept in mind: all three elements are directly applicable with all material models while the latter element is restricted to material models with decoupled isochoric and volumetric behavior. Nevertheless, in nearly incompressible rubber elasticity or in nearly incompressible metal elastoplasticity an isochoric-volumetric decoupled material behavior can be assumed for most practical applications and the SRI method can be employed without any disadvantage.

Our aim is to discuss the extension of the SRI method to finite deformation elastoplasticity resp. elasto-viscoplasticity and use it in the fully non-linear regime. The general motivation to come back to this rather well known strategy is its simplicity and the experience from large industrial computations that in rather refined meshes the bending behavior is far less important than the capabilities for almost incompressible deformations and the robustness of the element. Thus the major points are to show, if an efficient but reliable element can be achieved. In section 2 the basic relations for continuum-mechanics are introduced. In sections 3 and 4 the finite plastic case and the finite viscoplastic case are treated. It is shown that this includes also the pure finite elastic case. In contrast to Liu *et al.* (1992; 1994), a formulation in principal stretches instead of invariants is employed. In section 5 the numerical treatment of the additive split of the stress and moduli tensors is briefly described in order to allow a separate integration of the deviatoric and volumetric terms. In section 7 some material laws are introduced and numerical examples are given. Our focus is on the results obtained with the SRI element compared to the Q1, Q1/P0 (identical to $\bar{\boldsymbol{F}}_{\mathrm{Nag}}$) and $\bar{\boldsymbol{F}}_{\mathrm{Mor}}$ elements in elastoplastic and elastoviscoplastic applications. In contrast to these elements with solely modified volumetric part the EAS element contains modified strains, which are not restricted to the volumetric part only. However, this is not discussed in the 3D continuum examples, but the EAS-strategy is applied to the so-called solid-shell elements with enhancements for the shear

part and for the thickness direction which are necessary to achieve correct solutions for shell type applications. Section 8 concludes with the essential results.

2. Basic relations

As is well-known, using the finite element method for non-linear structural analysis an iterative global solution procedure has to be performed, mostly with a Newton-Raphson scheme. This solution procedure involves the computation of the residuum and the consistent linearization of the equilibrium equations at the current configuration. Herein the stress tensor and tangent moduli tensor have to be derived from the material law. In the following our focus is on these two tensors exclusively to set the environment to treat the large deformation case properly. First a spatial description is adopted and then extended to the total material description.

Using a spatial description the Kirchhoff stress tensor $\boldsymbol{\tau}$ and the Almansi strain tensor $\boldsymbol{e}$ are the conjugate stress and strain measures. The spatial tangent moduli tensor c relates the increment of the Kirchhoff stress tensor to the increment of the Almansi strain tensor $\Delta\tau = c\colon \Delta\boldsymbol{e}$. Due to isotropy the spectral decompositions of these tensors yield the identical spatial base eigenvectors $\boldsymbol{n}_i$. These eigenvectors result from the spectral decomposition of the left Cauchy-Green tensor $\boldsymbol{b} = \boldsymbol{F} \cdot \boldsymbol{F}^T$, where $\boldsymbol{F}$ denotes the deformation gradient. The deformation gradient is a pure kinematic measure, that can be computed without the knowledge of the material law. Therefore the spatial eigenvectors are as well computable without the knowledge of the material law.

The spectral representations of the spatial stress and moduli tensor are given in Table I. Due to the assumption of isotropy only the principal stresses τ_i and the moduli c_{iijj} and c_{ijij} depend on the material law.

1. Compute $\boldsymbol{F}$ and spatial eigenvector base $\boldsymbol{n}_i$
2. Compute components τ_i, c_{iijj}, c_{ijij} (as described in section 3)
3. Choose spatial or total material configuration:
   spatial → Set $\boxed{\boldsymbol{m}_i = \boldsymbol{n}_i}$
   material → Compute $\boldsymbol{F}^{-1}$ and set $\boxed{\boldsymbol{m}_i = \boldsymbol{F}^{-1} \cdot \boldsymbol{n}_i}$
4. Compute stress tensor and moduli tensor of chosen configuration:

$$\left.\begin{array}{l}\text{spatial} \rightarrow \boldsymbol{\tau} \\ \text{material} \rightarrow \boldsymbol{S}\end{array}\right\} = \sum_{i=1}^{3} \tau_i \boldsymbol{m}_i \otimes \boldsymbol{m}_i,$$

$$\left.\begin{array}{l}\text{spatial} \rightarrow c \\ \text{material} \rightarrow \mathbb{C}\end{array}\right\} = \sum_{i,j=1}^{3} c_{iijj} \boldsymbol{m}_i \otimes \boldsymbol{m}_i \otimes \boldsymbol{m}_j \otimes \boldsymbol{m}_j + \sum_{i \neq j} c_{ijij} \boldsymbol{m}_i \otimes \boldsymbol{m}_j \otimes (\boldsymbol{m}_i \otimes \boldsymbol{m}_j + \boldsymbol{m}_j \otimes \boldsymbol{m}_i)$$

Note: The additive deviatoric-volumetric split of the tensors is obtained using the split of the components

Table I.
Spatial-material transformation algorithm

Now the focus is on the total material description, that is based on the 2. Piola-Kirchhoff stress tensor $\boldsymbol{S}$ and the Green strain tensor $\boldsymbol{E}$. The total material moduli tensor $\mathbb{C}$ relates the increment of the 2. Piola-Kirchhoff stress tensor to the increment of the Green strain tensor $\Delta \boldsymbol{S} = \mathbb{C} : \Delta \boldsymbol{E}$. The increments of the stress and strain tensors of the material description can be determined from the spatial description by so-called pull-back transformations (Marsden, 1983):

$$\Delta \boldsymbol{E} = \boldsymbol{F}^T \cdot \Delta \boldsymbol{e} \cdot \boldsymbol{F}, \ \Delta \boldsymbol{S} = \boldsymbol{F}^{-1} \cdot \Delta \boldsymbol{\tau} \cdot \boldsymbol{F}^{-T}. \tag{1}$$

Using these transformations the material description as given in Table I can be derived. As known from the spatial description only the stress components τ_i and the moduli c_{iijj} and c_{ijij} depend on the material law, while the base vectors $\boldsymbol{F}^{-1} \cdot \boldsymbol{n}_i$ remain independent of the material law.

3. Finite elastoplasticity and the additive split

This sections deals with the determination of the stresses τ_i and the moduli c_{iijj} and c_{ijij} under the assumption of isotropic elastoplasticity at finite deformations. Following Kröner (1960), Lee and Liu (1967) and Lee (1969) for the kinematics of the deformation a multiplicative split of the deformation gradient $\boldsymbol{F} = \boldsymbol{F}^e \cdot \boldsymbol{F}^p$ into an elastic and a plastic part is supposed. This split involves the introduction of the determinant $J^e = \det \boldsymbol{F}^e$ of the elastic deformation gradient that measures the local elastic change of volume. In spectral decompositions the principal elastic stretches λ_i^e, the isochoric principal elastic stretches $\hat{\lambda}_i^e = (J^e)^{-1/3} \lambda_i^e$ and their logarithms ϵ_i^e, $\hat{\epsilon}_i^e$ are introduced as well (see Flory, 1961).

Further derivations in this section follow rather closely the form given by Simo and Armero (1992), Wriggers *et al.* (1996) and Reese and Wriggers (1997), to which we refer for details (see also Doll, 1998). In the following, only the aspects that are necessary for the further development are described.

The starting point of our development in isotropic finite elastoplasticity is the additive split of the energy function:

$$W(\epsilon_1^e, \epsilon_2^e, \epsilon_3^e, \xi) = \hat{W}(\hat{\epsilon}_1^e, \hat{\epsilon}_2^e, \hat{\epsilon}_3^e) + U(J^e) + W^p(\xi), \tag{2}$$

which consists of three parts: an isochoric elastic part $\hat{W}$, a volumetric elastic part U and a plastic part W^p. The plastic part depends on the scalar internal state variable ξ (equivalent plastic strain) and represents the isotropic plastic hardening behavior of the material.

To define the range of elastic deformation a decoupled yield condition:

$$\phi(\tau, q) = \phi_1(\tau) - \phi_2(q) \leq 0 \text{ with } \partial_\tau \phi = \operatorname{dev} \partial_\tau \phi, \ \operatorname{tr} \partial_\tau \phi = 0 \tag{3}$$

in Kirchhoff stress space is assumed (here and in further considerations ∂ denotes the first partial derivative with respect to the indicated variable and ∂^2 denotes the second partial derivative). The first part, $\phi_1 = \phi_1(\boldsymbol{\tau}) = \phi_1(\tau_1, \tau_2, \tau_3)$, here restricted to isotropic material behavior, represents the dependency on

the stress derived by $\boldsymbol{\tau} = 2b^e \cdot \partial_{b^e} W = 2\partial_{b^e} W \cdot b^e$ with b^e representing the elastic left Cauchy-Green tensor (see, for example, Coleman and Noll, 1963; Coleman and Gurtin, 1967; Simo, 1992). The second part ϕ_2 includes the isotropic hardening law derived by $q = \partial_\xi W$, (see, for example, Lemaitre and Chaboche, 1990). The yield condition must be fulfilled in a strong sense. As additional constraint the deviatoric character $(3)_{2,3}$ of the yield condition (as in metal plasticity) is supposed, which is essential for our development.

The associated plastic evolution equations follow from the principle of maximum internal dissipation, first introduced by von Mises (1928). The evolution equations are derived using the Kuhn-Tucker conditions (see Luenberger, 1984) and integrated with the well-known elastic predictor (intermediate configuration fixed, current configuration moved) plastic corrector (intermediate configuration moved, current configuration fixed) two step algorithm (see, for example, Simo and Taylor, 1985). The elastic predictor results in the trial elastic logarithmic stretches $\epsilon_i^{e,trial}$ and the trial equivalent plastic strain ξ^{trial}. The plastic corrector results in the additive update formula:

$$\epsilon_i^e = \epsilon_i^{e,trial} - \Delta\gamma \partial_{\tau_i}\phi \text{ and } \xi = \xi^{trial} - \Delta\gamma\partial_q\phi. \tag{4}$$

The discrete plastic multiplier $\Delta\gamma$ scales the plastic flow and ensures the fulfillment of the yield condition (3), which is included in the discrete Kuhn-Tucker conditions:

$$\phi(\tau, q) \leq 0,\ \Delta\gamma \geq 0,\ \Delta\gamma\phi(\boldsymbol{\tau}, q) = 0. \tag{5}$$

Details concerning this topic are discussed in Simo and Armero (1992) and Schellekens and Parisch (1994).

Combining equations (3) and (4) with the definitions of the logarithmic elastic stretches the essential results for our further considerations are as follows:

$$\begin{aligned} &\partial_{\tau_1}\phi + \partial_{\tau_2}\phi + \partial_{\tau_3}\phi = 0,\ \epsilon_1^e + \epsilon_2^e + \epsilon_3^e = \epsilon_1^{e,trial} + \epsilon_2^{e,trial} + \epsilon_3^{e,trial}, \\ &J^e = J^{e,trial},\ \hat{\epsilon}_i^e = \hat{\epsilon}_i^{e,trial} - \Delta\gamma\partial_{\tau_i}\phi. \end{aligned} \tag{6}$$

Due to the deviatoric character of the yield condition $(6)_1$, the sum $(6)_2$ of the three elastic logarithmic stretches is unaffected by the plastic correction. The elastic change of volume $(6)_3$ remains constant during plastic correction and the plastic correction $(6)_4$ is purely deviatoric.

The application of the stress formula on the energy function (2) leads to the following decoupled principal stress components:

$$\tau_i = \tau_i^{dev} + \tau^{vol},\ \tau_i^{dev} = \partial_{\hat{\epsilon}_i^e}\hat{W} - \frac{1}{3}\sum_{k=1}^{3}\partial_{\hat{\epsilon}_k^e}\hat{W},\ \tau^{vol} = \left[J^e\partial_{J^e}U\right]_{J^e=J^{e,trial}}. \tag{7}$$

Using the results $(6)_3$ and $(6)_4$ it is evident that the volumetric stress is unaffected by the plastic correction but the deviatoric stress depends on the plastic correction.

The application of the procedure proposed in Reese and Wriggers (1997) on the energy function (2) leads to the decoupled principal components:

$$
\begin{aligned}
& c_{iijj} = c^{dev}_{iijj} + c^{vol}_{iijj},\ c^{dev}_{iijj} = -2\delta_{ij}\tau^{dev}_i + \partial_{\epsilon^{e,trial}_j}\tau^{dev}_i,\ c^{vol}_{iijj} = -2\delta_{ij}\tau^{vol} + \partial_{\epsilon^{e,trial}_j}\tau^{vol}, \\
& c_{ijij} = c^{dev}_{ijij} + c^{vol}_{ijij}, \\
& c^{dev}_{ijij} = [(\hat{\lambda}^{e,trial}_i)^2 - (\hat{\lambda}^{e,trial}_j)^2]^{-1}[(\hat{\lambda}^{e,trial}_j)^2\tau^{dev}_i - (\hat{\lambda}^{e,trial}_i)^2\tau^{dev}_j], \\
& c^{vol}_{ijij} = -\tau^{vol}, \\
& \text{limit case}: \ \hat{\lambda}^{e,trial}_i \to \hat{\lambda}^{e,trial}_j : \ c^{dev}_{ijij} = \frac{c^{dev}_{iiii} - c^{dev}_{jjii}}{2},\ c^{vol}_{ijij} = \frac{c^{vol}_{iiii} - c^{vol}_{jjii}}{2}
\end{aligned}
\tag{8}
$$

of the moduli tensor. It must be emphasized, that the additive split of the stresses (7) leads directly to the additive split of the stress derivatives:

$$
\begin{aligned}
\partial_{\epsilon^{e,trial}_j}\tau_i &= \partial_{\epsilon^{e,trial}_j}\tau^{dev}_i + \partial_{\epsilon^{e,trial}_j}\tau^{vol}, \\
\partial_{\epsilon^{e,trial}_j}\tau^{dev}_i &= \partial_{\epsilon^{e,trial}_i}\tau^{dev}_j = \text{no explicit expression}, \\
\partial_{\epsilon^{e,trial}_j}\tau^{vol} &= \tau^{vol} + \left[(J^e)^2\partial^2_{J^eJ^e}U\right]_{J^e=J^{e,trial}}
\end{aligned}
\tag{9}
$$

which appear in the moduli c_{iijj}. The volumetric part in equation $(9)_3$ is unaffected by the plastic correction. Because the volumetric stress $(7)_3$ is explicitly dependent on the trial elastic stretches, the derivation can be carried out and the explicit expression $(9)_3$ can be obtained. Due to the plastic correction, no explicit expression can be obtained for the elastoplastic deviatoric part $(9)_2$. This problem is the subject of the following paragraph.

To obtain a quadratic convergence rate within the global Newton-Raphson solution scheme, the linearization of the material law must include the elastic predictor-plastic corrector algorithm (Simo *et al.*, 1985; Simo and Taylor, 1986). This linearization (see, for example, Simo and Armero, 1992), involves the computation of the derivative $\partial_{\epsilon^{e,trial}_j}\tau_i$, that includes a modified modulus:

$$
[(\partial^2_{\underline{\epsilon}^e\underline{\epsilon}^e}W)^{-1} + \Delta\gamma\partial^2_{\underline{\tau}\,\underline{\tau}}\phi]^{-1} \text{ with } \underline{\epsilon}^e = [\epsilon^e_1, \epsilon^e_2, \epsilon^e_3]^T,\ \underline{\tau} = [\tau_1, \tau_2, \tau_3]^T. \tag{10}
$$

Due to the decoupled energy function (2), the second derivative:

$$
\partial^2_{\underline{\epsilon}^e\underline{\epsilon}^e}W = \partial^2_{\underline{\epsilon}^e\underline{\epsilon}^e}\hat{W} + \partial^2_{\underline{\epsilon}^e\underline{\epsilon}^e}U \tag{11}
$$

can be decoupled too. Inserting equation (11) in equation $(10)_1$ the inversion

destroys the advantage of an additive split, which was the starting point in equation (11). Therefore no explicit additively decoupled expression $(9)_1$ is obtainable, especially no explicit expression for the deviatoric part $(9)_2$ can be obtained. However, the deviatoric part can be determined numerically by a rearrangement of equation $(9)_1$:

$$\partial_{\epsilon_j^{e,trial}} \tau_i^{dev} = \partial_{\epsilon_j^{e,trial}} \tau_i - \partial_{\epsilon_j^{e,trial}} \tau^{vol}. \tag{12}$$

The explicit expression for $\partial_{\epsilon_j^{e,trial}} \tau^{vol}$ is given in $(9)_3$ and can be evaluated in a straightforward fashion, whereas $\partial_{\epsilon_j^{e,trial}} \tau_i$ is numerically computable following standard procedures. Then, with the knowledge of (12), all terms in (8) are computable. Finally, inserting the decoupled components (7), (8) into the stress and moduli tensors given in Table I results in a decoupling of these tensors, i.e. $\boldsymbol{\tau} = \boldsymbol{\tau}^{dev} + \boldsymbol{\tau}^{vol}$, $c = c^{dev} + c^{vol}$ and $\boldsymbol{S} = \boldsymbol{S}^{dev} + \boldsymbol{S}^{vol}$, $\mathbb{C} = \mathbb{C}^{dev} + \mathbb{C}^{vol}$ (see also, for a special case of a material law, Simo, 1988).

Finite elasticity. The relations mentioned above include the pure elastic case by simply setting $\boldsymbol{F}^p = 1$, $\Delta\gamma = 0$, $\epsilon_i^{e,trial} = \epsilon_i^e$ and $\xi = 0$ (for further details see, for example, Chadwick and Ogden, 1971; Ogden, 1984; Reese, 1994; Crisfield, 1997).

4. Extension to finite elastoviscoplasticity

The finite elastoviscoplastic case is contained in the basic relations mentioned above by application of a few modifications. All inelastic deformations are now pure viscoplastic deformations, i.e. $\boldsymbol{F}^{vp}$ replaces $\boldsymbol{F}^p$ in the multiplicative split of the deformation gradient. It should be noted, that time dependent viscous material behavior occurs only in the presence of plastic yielding. Our formulation is of the Perzyna-type viscoplasticity (see Perzyna, 1963; 1971) and is motivated by the considerations of Miehe (1993). For an extensive discussion of algorithms we refer to Runesson *et al.* (1999).

In contrast to the plastic case mentioned above, the evolution equations are now derived using the penalty method, described in Luenberger (1984) as an approximate method. The fulfillment of the yield condition (3) is enforced by a penalty term:

$$\frac{\tau_0^2}{\eta}\beta(\phi^+(\boldsymbol{\tau}, q)) \text{ with } \phi^+(\boldsymbol{\tau}, q) = \max[0, \phi(\boldsymbol{\tau}, q)/\tau_0] \quad \text{and } \partial_{\phi^+}\beta(\phi^+)|_{\phi^+=0} = 0 \tag{13}$$

in the maximization process of the internal dissipation. The constant positive scalar stress $\tau_0 > 0$, here the first yield stress, is used to make the yield condition dimensionless. The penalty factor τ_0^2/η of the dimension of the internal dissipation ensures the exactness of the method, if the positive scalar viscosity parameter tends to zero, i.e. $\eta \to 0$. For the description of the viscoplastic material behavior the dimensionless penalty function β has to be prescribed. The integration of the evolution equations is carried out with the standard predictor-corrector

algorithm and leads to the identical update formula (4) as in the plastic case. The corresponding viscoplastic multiplier can be computed from the residual equation:

$$R_B = -\frac{\eta}{\Delta t}\Delta\gamma + \tau_0 \partial_{\phi^+}\beta(\phi^+) = 0, \tag{14}$$

that follows directly by rearrangement of the loading condition:

$$\Delta\gamma = \frac{\tau_0}{\eta}\Delta t \partial_{\phi^+}\beta(\phi^+). \tag{15}$$

The residual equation (14) replaces the discrete Kuhn-Tucker conditions (5) of the plastic case. The time increment Δt shows the explicit time dependency of the formulation. In general the evaluation of the viscoplastic multiplier $\Delta\gamma$ must be performed iteratively. Using the residual equation instead of the loading condition circumvents the ill-conditioning known from some other algorithms for viscoplasticity in the limit case of rate independent plasticity when $\eta \to 0$ (for details, see Doll, 1998 and Runesson *et al.*, 1999, resp.). Inserting the viscoplastic multiplier instead of the plastic multiplier in the equations mentioned above allows to switch from the plastic formulation to the viscoplastic formulation.

5. Numerical treatment of the additive split

The additive split of the stress tensor and the moduli tensor permits a different treatment of the deviatoric and volumetric part numerically. In the context of finite element calculations the use of different numerical integration schemes is proposed in (Liu *et al.*, 1992; 1994). Full numerical integration is employed for the deviatoric terms while selective reduced integration is employed for the volumetric terms of the internal force vector and the tangent stiffness matrix. This procedure avoids volumetric locking phenomena, which occur in the treatment of nearly incompressible elasticity, e.g. rubber with ratio bulk modulus/shear modulus $\gg 1$, in combination with pure low-order displacement based finite elements. Performing reduced integration one order below full integration is recommended.

To assess the SRI scheme in practical applications for elastoviscoplastic material the decoupled stress tensors and moduli tensors are implemented with a three-dimensional non-linear eight-node displacement Q1 element (see, for example, Liu *et al.*, 1994), and with a number of non-linear four(eight)-node displacement solid shell elements from which the so-called ANS3Dq and the eas3Dq elements are taken as typical representatives (see Hauptmann, 1997; Harnau *et al.*, 2000). The Q1 element is formulated with respect to the spatial configuration and the ANS3Dq resp. the eas3dq elements are formulated with respect to the total material configuration. At each integration point the history variables (here $\boldsymbol{b}^e$, ξ in the plastic and viscoplastic case) must be stored. For example, performing selective reduced integration for the Q1 element one integration point at the element center has to be added to the eight standard Gauss-points. The notations: Q1/d8v8 is the fully integrated element with

$2 \times 2 \times 2$ integration for all terms (identical to the Q1 element). Q1/d8v1 means selective reduced integration, i.e. full $2 \times 2 \times 2$ integration for the deviatoric part and reduced $1 \times 1 \times 1$ integration for the volumetric part. It should be mentioned, that due to plastic incompressibility $J = J^e = J^{e,trial}$ the volumetric part can be computed without return mapping, i.e. without knowledge of $\boldsymbol{b}^e$, ξ.

6. Removal of artificial instabilities by a simple mixed integration

From numerical examples it is known that under certain loading conditions using the SRI elements artificial instabilities occur, so-called hour-glass modes. Such an artifact was also observed by Wriggers and Reese (1996) for the EAS-elements under certain loading conditions. Glaser and Armero (1997) suggest a procedure to overcome this deficiency, however the effort needed seems to be rather high and the removal is only guaranteeing a stable procedure. This is also the case for the suggestions of Reese *et al.* (1999) and Reese and Wriggers (1999).

The task now is how to avoid hour-glassing, thus gaining stability back with little effort. It is known, that the standard Q1 element, here identical with the Q1/d8v8 element, shows no hour-glassing but volumetric locking. Thus a mixed selective integration rule combining the reduced volumetric locking behavior of the Q1/d8v1 element with the full integration of the Q1/d8v8 element removes the instability but also reintroduces some locking back into the problem. Mixed integration rule means that the selectively reduced integrated volumetric part is multiplied by ζ and added to the volumetric part fully integrated at the eight Gauss points and multiplied by $(1 - \zeta)$, see similar approach by Moran *et al.* (1990). The latter part should lead to a stabilization of the stiffness matrix and should preserve its rank. To obtain a quadratic convergence rate within the global Newton-Raphson solution scheme the mixed integration is employed in the computation of the internal force vector as well as in the computation of the tangent stiffness matrix. The volumetric weight factor $\zeta \in [0, 1]$ sets the limits for $\zeta = 1$ to the Q1/d8v1 formulation and for $\zeta = 0$ to the Q1/d8v8 formulation. The mixed integrated element Q1/d8v1-ζ is denoted by the attachment of the letter ζ. It must be noted that the stabilized Q1/P0-element of Crisfield and Norris (1999) appears to rely also on a similar "stabilization" factor. This factor has to be chosen depending on the problem, which could be done investigating eigenvalues; however, the simplicity remains by a heuristically chosen constant factor allowing an efficient procedure. It is a definite disadvantage that the value for the weight factor has to be chosen before the computation is started, though it is in principle problem dependent and usually not known in advance. In particular the incompressibility indicator, denoted as K/μ^* in section 7.2 has some influence on the size of this volumetric weight factor. Standard values are discussed in the various examples following and ways of how to proceed in different cases can be deduced.

Removal of hour-glassing by modification of the $\bar{\boldsymbol{F}}$ elements

As a further alternative the modification $\bar{\boldsymbol{F}}^* = (\bar{J}/J)^{z/3}\boldsymbol{F}$ with $z \in [0, 1]$ is proposed here to obtain hour-glass free $\bar{\boldsymbol{F}}$ elements. This modification leads to a mixed determinant $\bar{J}^* = \det \bar{\boldsymbol{F}}^* = \bar{J}^z J^{1-z}$. The sum of the exponents is

always 1. Using $z = 1$ the original formulation with constant determinant $\bar{J}^* = \bar{J}$ over the whole element is identically recovered. Using $z = 0$ results in the standard Q1 element. This approach is similar to the selectively mixed integrated element Q1/d8v1-ζ in the sense, that one part of the volumetric behavior, here $\bar{J}^z$, is treated as constant while the other part of the volumetric behavior, here J^{1-z}, is treated as non-constant. Looking at the value ζ (see the numerical examples in section 7) it seems to be a good recommendation to choose the value z near one, such that within the element the constant part $\bar{J}$ dominates over the non-constant part J, e.g. $z = 9/10$ yields $\bar{J}^* = \bar{J}^{9/10} J^{1/10}$. The proposed modification can be interpreted as multiplicative version of the modification suggested by Moran *et al.* (1990). However, the proposed modification is neither implemented nor tested yet.

7. Numerical examples

In the following first the used material laws are introduced. Then a number of numerical simulations is carried out to demonstrate the merits and limits of the SRI method and the mixed integration in the case of elastoviscoplasticity. It should be mentioned in advance, that in all numerical analyses a quadratic convergence of the global Newton-Raphson scheme is observed, unless otherwise noted.

7.1 Used material laws

To describe the elastoviscoplastic material, which is the most general material considered here, a decoupled energy function (2), a yield condition (3) and a penalty function (13) have to be prescribed. The elastoplastic material is obtained by setting the viscosity to zero. The elastic material is obtained by setting the first yield stress to infinity. All functions, that describe the non-linear behavior of the materials considered in the numerical examples, are given in the following.

The energy function I with

$$\begin{aligned} &\hat{W} = \mu[(\hat{\epsilon}_1^e)^2 + (\hat{\epsilon}_2^e)^2 + (\hat{\epsilon}_3^e)^2],\ U = K(\ln J^e)^2/2, \\ &W^p = H\xi^2/2 + (\tau_\infty - \tau_0)\xi + \delta^{-1}(\tau_\infty - \tau_0)\exp(-\delta\xi) \text{ with } \delta > 0 \end{aligned} \tag{16}$$

is taken from (Simo, 1992) . The elastic terms $\hat{W}$ and U are as introduced by Hencky (1933). The plastic term W^p yields a saturation type hardening law, see Simo *et al.* (1985) and Simo (1988). Herein the constants are the shear modulus μ, the bulk modulus K, the first yield stress τ_0, the saturation yield stress τ_∞, the linear hardening modulus H and the saturation exponent δ. For the energy function (16) in combination with the von Mises yield condition, introduced in equation (18), an explicit expression for $\partial_{\epsilon_j^{e,trial}} \tau_i$ can be derived (see Simo and Armero, 1992). Because the derivative $\partial_{\epsilon_j^{e,trial}} \tau^{vol} = K$ is known, an explicit expression for $\partial_{\epsilon_j^{e,trial}} \tau_i^{dev}$ is obtainable from equation (12).

The energy function II with

$$\begin{aligned}
\hat{W} &= \sum_{m=1}^{3} \frac{\mu_m}{\alpha_m} [\exp(\alpha_m \hat{\epsilon}_1^e) + \exp(\alpha_m \hat{\epsilon}_2^e) + \exp(\alpha_m \hat{\epsilon}_3^e) - 3] \\
&\quad \text{with } \mu_m \alpha_m > 0, \ \sum_{m=1}^{3} (\mu_m \alpha_m) = 2\mu, \\
U &= K[(\theta+1)^{-1} (J^e)^{\theta+1} + (\Omega-1)^{-1} (J^e)^{-(\Omega-1)}](\theta+\Omega)^{-1} \\
&\quad - K(\theta+1)^{-1}(\Omega-1)^{-1} \\
&\quad \text{with } \theta > 0, \ \Omega > 1, \\
W^p &= H\xi^2/2 + (a+1)^{-1} H_2 \xi^{(a+1)}
\end{aligned} \tag{17}$$

contains a three-term isochoric elastic energy function $\hat{W}$ of the Ogden type (Ogden, 1972a; 1972b). Herein the isochoric elastic stretches replace the elastic stretches of the original function. The volumetric elastic energy function U is proposed in Doll and Schweizerhoff (1997). The elastic parts $\hat{W}$ and U contain the moduli μ_m and the exponents α_m, θ and Ω. The conditions for these constants of the energy function occur due to physical considerations. The plastic term W^p in function (17) is taken from Reese and Wriggers (1997). It consists of a linear hardening law with a non-linear extension (hardening modulus H_2 and exponent a).

The yield condition

$$\begin{aligned}
\phi &= \|\text{dev}\boldsymbol{\tau}\| - \sqrt{2/3}\,(\tau_0 + q) \le 0 \\
&\quad \text{with } \|\text{dev}\,\boldsymbol{\tau}\| = [(\tau_1^{dev})^2 + (\tau_2^{dev})^2 + (\tau_3^{dev})^2]^{1/2}
\end{aligned} \tag{18}$$

covers the case of plasticity with isotropic hardening (τ_0 ... first yield stress, q ... isotropic hardening law) and is well-known from metal plasticity. The deviatoric character of the yield condition (18), which is essential for our development, is evident.

The penalty function

$$\beta(\phi^+) = \frac{1}{1+\omega} [\phi^+]^{1+\omega} \tag{19}$$

goes back to Perzyna (1963; 1966) and leads to a residual equation (14) of the exponential type with exponent ω. It should be noted, that the rate independent plastic case is identically recovered without ill-conditioning, if the exponent $\omega = 1$ and the viscosity $\eta \to 0$ are chosen.

7.2 Compression of a block

This example is adopted from van den Bogert *et al.* (1991), Liu *et al.* (1992; 1994) dealing with rubber-like materials. Our purpose is to show the application of

the SRI scheme to the finite deformation elastoplastic case. Results concerning the nearly incompressible elastic case are omitted with reference to Liu *et al.* (1992; 1994).

The compressed block considered here is of the dimension $10 \times 10 \times 10$mm. The material behavior is prescribed by the energy function I given in equation (16) and the yield condition (18). The material data are given in Table II. The resulting isotropic plastic hardening law is linear.

The computations are performed with regular discretizations of $n \times n \times n$ brick elements per eighth of the block taking advantage of symmetry in three planes (see Figure 1(a)). The compression is imposed by a constant vertical displacement of the upper surface with the horizontal displacements fixed. On the symmetry planes only in-plane sliding is allowed. The total vertical compression of 20 percent is attained after ten displacement increments, each of 2 percent. As seen from Figure 2 the load-compression curves for the Q1/d8v8 element with all meshes are well above the curves for the Q1/d8v1 element, i.e. as expected the fully integrated element behaves stiffer than the selectively reduced integrated element. Mesh refinement from $n = 4$ to 8 and 16 lowers the load-compression curves of the Q1/d8v8 element while refinement from $n = 4$ to 8 does not lead to significantly different curves for the Q1/d8v1 element. Already coarse meshes give rather accurate solutions in combination with the Q1/d8v1 element.

For $n = 16$ the Q1/d8v1 element does not converge in the global solution scheme. For this problem the Q1/d8v1 element seems to be more sensitive than the Q1/d8v8 element. The reason is that in the fine mesh the fixed size of the displacement increments is large in relation to the decreased characteristic single element length, which causes large single element deformations and as a

Table II.
Material data for the compressed block

	Constant					
	μ ($\equiv$ N/mm^2)	K ($\equiv$ N/mm^2)	τ_0 ($\equiv$ N/mm^2)	H ($\equiv$ N/mm^2)	τ_∞ ($\equiv$ N/mm^2)	δ
Value	80.1938	164.21	0.45	0.1	0.45	10^{10}

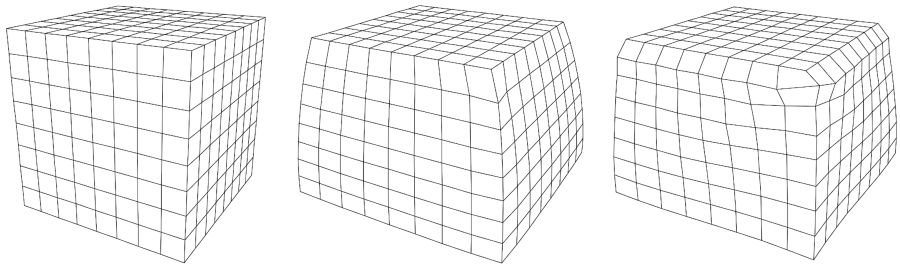

(a) eighth of initially undeformed block

(b) eighth of deformed block at 20% compression, Q1/d8v8 element

(c) eighth of deformed block at 20% compression, Q1/d8vl element

Figure 1.
Compressed block, $8 \times 8 \times 8$ element mesh

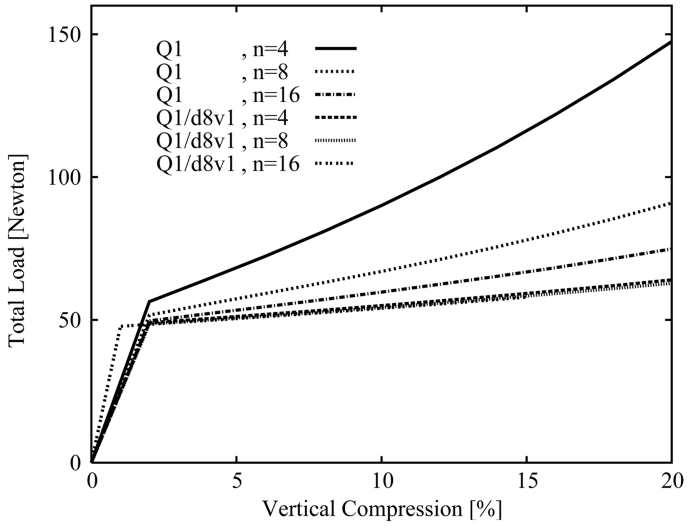

Figure 2.
Compressed block. Load versus compression obtained with the Q1/d8v8 element and Q1/d8v1 element for various meshes

consequence a reduction of the convergence rate. For the finest mesh small displacement increments of 1 percent lead to a convergent solution in the beginning of the analysis up to 15 percent. In the interesting region the curve is nearly indistinguishable from the curves for the coarser meshes with $n = 4$, 8 and Q1/d8v1. The steeper slope of the curve in the first load step and the kink at 1 percent are only results of the reduced step length and are not of further interest. For both increments of 1 percent and 2 percent the first load step falls directly into the plastic region, i.e. the kink in the curves does not display the elastic plastic limit. The reason for the brake-down of the solution beyond 15 percent compression is the loss of convexity of the deformed corner element geometry, which is depicted in Figure 1(c) for the coarser mesh $n = 8$. In the considered compression range up to 20 percent this effect does not occur using the Q1/d8v8 element, because the inherent volumetric locking prevents such large deformations of the corner element, see Figure 1(b).

Alternative analyses are carried out using the $\bar{\boldsymbol{F}}_{Mor}$ element described in Section 1. Within the numerical accuracy these results are indistinguishable from the results obtained with the Q1/d8v1 element and therefore omitted in Figures 1 and 2. As already described the general $\bar{\boldsymbol{F}}$-formulation is based on a modified deformation gradient with a constant determinant $\bar{J}$ over the whole element. This modification does not influence the deviatoric stress and moduli tensors, i.e. these tensors are identical for both element formulations. Especially, for $\bar{\boldsymbol{F}}_{Mor} = (\bar{J}/J)^{1/3}\boldsymbol{F}$ with $J = \det \boldsymbol{F}$ and $\bar{J} = J_0 = \det \boldsymbol{F}_0$ at the element center the Q1/d8v1 formulation is identically recovered for the decoupled energy functions. Then also the volumetric stress and moduli tensors are identical for both element formulations. For the pure elastic case the identity $\bar{J} = J_0 = J_0^e$ is straightforward. For the elastoplastic case with deviatoric plastic yielding this identity holds as well, because $J_0^p = \det \boldsymbol{F}_0^p = 1$

has to be taken into account. Using the Q1/P0 element, which is identical to the $\bar{\boldsymbol{F}}_{Nag}$ element, all results obtained with the Q1/d8v1 element can be confirmed within a small tolerance.

As mentioned above, the SRI scheme was used in Liu *et al.* (1992; 1994) for nearly incompressible elastic material behavior with $K/\mu \gg 1$, i.e. for a very large ratio of the bulk modulus and the shear modulus. The material constants taken from Table II yield a ratio $K/\mu \approx 2$ that is not as large; thus the elastic material is not close to being incompressible. The volumetric locking possibility, observed in our example, stems from the plastic material behavior, which is purely deviatoric and therefore totally incompressible. The plastic behavior reduces the "shear"-stiffness of the material. In the linear elastic case the shear modulus is defined as $\mu = \tau/\gamma$, where τ is the shear stress and γ is the elastic engineering shear strain. In the elastoplastic case (here for simplicity with the additive split of strains) this formula can be rewritten as $\mu^* = \Delta\tau/(\Delta\gamma^e + \Delta\gamma^p)$, where μ^* can be interpreted as "local elastoplastic" shear modulus. If plastic deformations are present, a small increase of $\Delta\tau$ normally yields a large increase of $\Delta\gamma^p$, i.e. μ^* becomes small. Using now K/μ^* as incompressibility indicator it is evident that K/μ^* can be large although K/μ is small.

7.3 Necking of a circular bar under extension

This example is adopted from Simo and Armero (1992), de Souza Neto *et al.* (1996), Simo (1992; 1988), Schellekens and Parisch (1994), Müller-Hoeppe (1990) among others. The geometry of the circular bar is chosen as follows: total length 53.334mm, radius 6.413mm at the ends of the bar, radius 6.105mm in the symmetry plane. Starting from the ends of the bar to the central symmetry plane, a linear reduction in the radius along the length is imposed. This geometric imperfection induces plastic yielding in the symmetry plane and avoids an initially homogeneous stress state. Simulations, where the necking of an initially geometric perfect bar is induced by the thermo-mechanical coupling, are considered, e.g. in Simo *et al.* (1993) and Miehe (1993), but are not the subject of the present contribution.

The material behavior is prescribed by the energy function I given in (16), the yield condition (18) and the penalty function (19). The material constants are given in Table III. The viscosity η with a unit Ns/mm^2, not contained in Table III, will be discussed later.

The following investigations are based on two different finite element meshes. Due to symmetry only one eighth of the bar has to be discretized. The

Table III.
Material data for the circular bar

	Constant						
	μ ($\equiv$ N/mm^2)	K ($\equiv$ N/mm^2)	τ_0 ($\equiv$ N/mm^2)	H ($\equiv$ N/mm^2)	τ_∞ ($\equiv$ N/mm^2)	δ	ω
Value	80.1938	164.21	0.45	0.12924	0.715	16.93	1

first mesh consists of 120 brick elements and is used for elastoviscoplastic investigations with variable viscosity η. The second mesh consisting of 960 brick elements is identical to the mesh considered in Simo (1992). Within the present contribution the focus is on the rate-independent plastic case (η very small) with special interest in the hour-glassing occurring at a certain loading state, which was also observed in Simo (1992) for the Q1/P0 element.

7.3.1 Necking problem using a coarse mesh with 120 elements. The discretization is shown in Figure 3(a). It consists of 12 brick elements in each cross section and ten brick elements in axial direction. Loading is applied by an extensional axial displacement w of the bar ends, where in-plane displacements are allowed. Here w is the elongation of the half specimen. Starting from time $t = 0$s up to time $t = 0.7$s the axial displacement $w = \dot{w}t$ is applied within 70 equal time steps $\Delta t = 0.01$s at a constant displacement rate of $\dot{w} = 10$mm/s (unit s means seconds). For $t > 0.7$s the axial displacement is held fixed at $w = 7$mm, such that viscous effects can lead to some relaxation. The time step size $\Delta t = 0.01$s remains unchanged then. Inertia effects are assumed to be negligible.

The subject of this investigation is to study the behavior of the Q1/d8v8 and Q1/d8v1 element formulations in combination with viscoplastic effects. In Figures 4 and 5 the total axial force in the bar is plotted versus the time. The curves obtained with the Q1/d8v8 element are shown in Figure 4. The curve related to the small viscosity parameter $\eta = 10^{-8}$ can be taken as the time independent plastic limit curve of the problem. All load curves for viscosities $\eta > 10^{-8}$ should be above this limit curve, because with larger viscosity parameters the load should be larger due to the viscous overstress. When η is chosen to 10^{-1} resp. 10^{-2} the relaxation process for $t > 0.7$s becomes clearly visible. However, for all considered viscosities the relaxed loads are fairly close to each other, some are nearly identical. The curves $\eta = 10^{-3} \ldots 10^{-8}$ are almost not distinguishable within the accuracy of the plot, i.e. the plastic limit case is already obtained for rather moderate viscosity parameters. As visible from the load curves in Figure 4 and the mesh in Figure 3(b), the fully integrated Q1/d8v8 element behaves very stiff and does not allow necking at all.

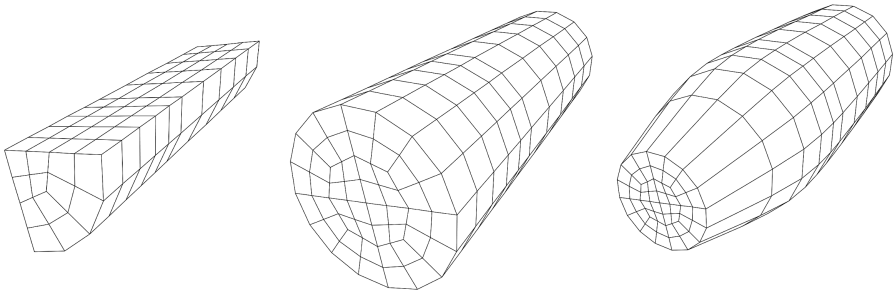

(a) eighth of initially undeformed specimen

(b) half of deformed specimen at $t = 0.7$s, Q1/d8v8 element, $\eta = 10^{-8}$

(c) half of deformed specimen at $t = 0.7$s, Q1/d8v1 element, $\eta = 10^{-8}$

Figure 3.
Necking bar, 120 element mesh

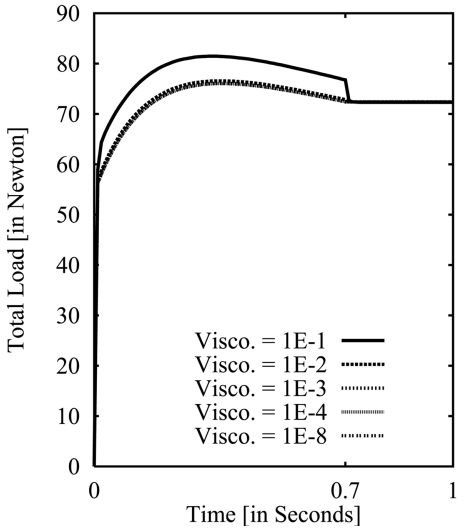

Figure 4.
Necking bar, 120 element mesh. Axial load versus time obtained with the Q1/d8v8 element for various viscosities η

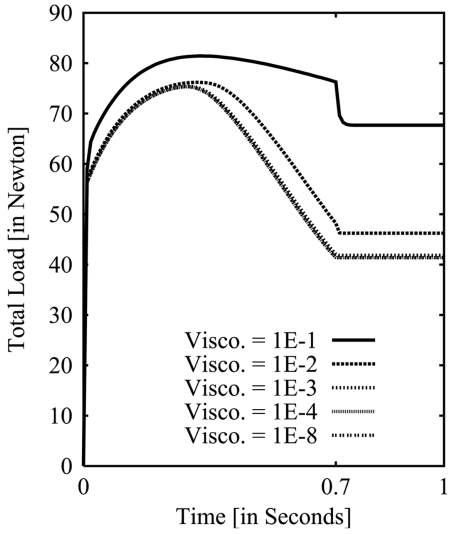

Figure 5.
Necking bar, 120 element mesh. Axial load versus time obtained with the Q1/d8v1 element for various viscosities η

The curves resulting from computations with the Q1/d8v1 element are shown in Figure 5. Now the necking phenomenon – a steep decrease of the load curve after the limit point is passed – can be described, as also shown in Figure 3(c). It must be noted, that the load curve of the time independent case $\eta = 10^{-8}$ compares very well to the results described in Simo (1992). The SRI method reduces volumetric locking correctly as the steep decreasing load curves show. It is also visible that the viscous effects appear to be more evident for the SRI computations than for the fully integrated element. For $t > 0.7$s the relaxation of the overstress is also larger than for the fully integrated counterpart.

Furthermore the curves obtained with different viscosity parameters are more distinct. In particular the loads after relaxation are different. In Figure 5 the curve for $\eta = 10^{-2}$ is not as close to the plastic limit curve as its counterpart in Figure 4. The curve for $\eta = 10^{-3}$ nearly coincides with the plastic limit curve in Figure 4, which is not the case for its counterpart in Figure 5. Using the 120 element mesh the results obtained with the Q1/d8v1 element do not exhibit any artificial instability (= hour-glassing) (see Figure 3(c) for the plastic case.

7.3.2 Necking problem using a fine mesh with 960 elements. The mesh, shown in Figure 6(a), consists of 48 elements in each cross section and 20 elements in axial direction with increased mesh density near the symmetry plane to capture the necking effects. Here the rate independent plastic case is considered. The viscosity $\eta = 10^{-6}$ is chosen to be very small, i.e. the used time increment size has no significant influence on the final results. Loading is applied by the following extensional axial displacement w of the bar ends: five equal increments $\Delta w = 0.56$mm up to $w = 2.8$mm, 15 equal increments $\Delta w = 0.08$mm up to $w = 4$mm and ten equal increments $\Delta w = 0.3$mm up to $w = 7$mm.

As the fully integrated Q1/d8v8 element cannot describe the necking phenomenon, only the selectively reduced integrated Q1/d8v1 element is used for the 960 brick element mesh. In Figure 7 the total axial force in the bar is plotted versus the elongation of the half specimen. The lowest curve is obtained using the pure Q1/d8v1 element. This curve is nearly identical to the curve obtained by Simo and Armero (1992) with the Q1/P0 element. As mentioned above, the $\bar{\boldsymbol{F}}_{Mor}$ element yields the same results as the Q1/d8v1 element, if isochoric-volumetric decoupling is assumed. All these elements, i.e. the Q1/P0 or $\bar{\boldsymbol{F}}_{Nag}$ element and the Q1/d8v1 or $\bar{\boldsymbol{F}}_{Mor}$ element, have one identical property: the volumetric terms in the element are treated as constant. Looking at the deformed mesh in Figure 6(b) it is evident, that the $\bar{\boldsymbol{F}}_{Mor}$ and Q1/d8v1 element show considerable hour-glassing from some deformation state on as is already known from the Q1/P0 element (see Simo, 1992). It seems also, that starting at the boundaries, where the element edges are held fixed (e.g. in the central symmetry plane of the bar), a rather fine mesh is necessary until hour-glassing

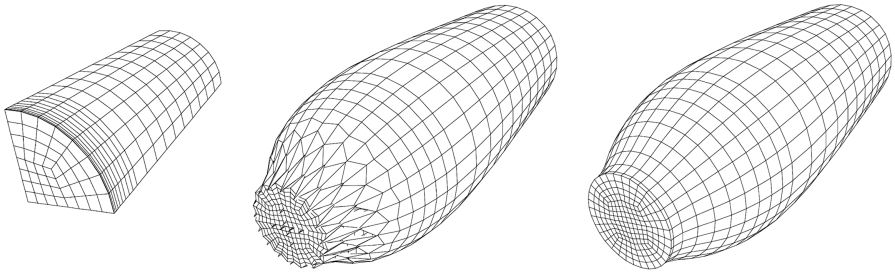

(a) eighth of initially undeformed specimen

(b) half of deformed specimen at $w = 7$mm, Q1/d8v1 element

(c) half of deformed specimen at $w = 7$mm, Q1/d8v1-0.99 element

Figure 6.
Necking bar, 960 element mesh

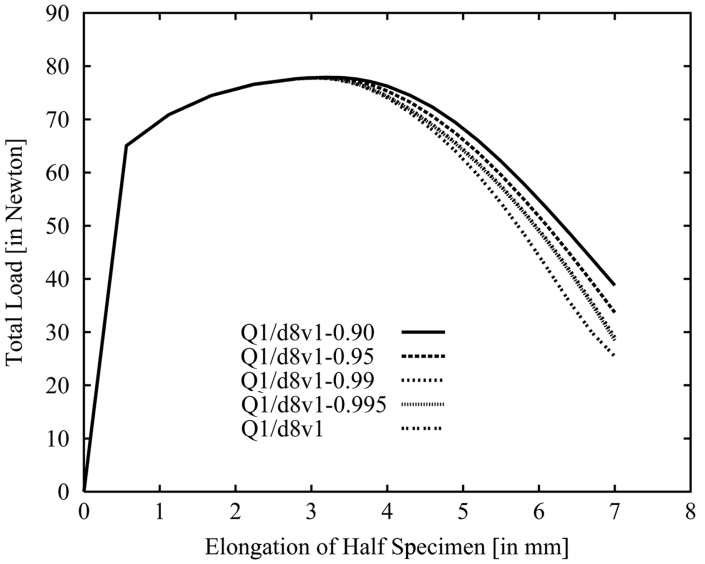

Figure 7.
Necking bar, 960 element mesh. Axial load versus elongation obtained with the Q1/d8v1-ξ element for various volumetric weight factors

can develop. It must be noted that the Q1/P0 elements show identical results up to $w = 5.8$mm, however, at larger elongation severe hour-glassing occurs and the final solution $w = 7$mm is not obtainable for the applied load increments.

In Figure 7 the load-elongation curves obtained with the mixed integrated element for values of $\zeta = 0.995, 0.99, 0.95, 0.9$ are plotted. Decreased weight factors ζ lead to increased element stiffness and vice versa. For all used ζ-values no hour-glassing occurs, i.e. the stabilization preserves clearly the rank of the stiffness matrix. Here the value $\zeta = 0.99$ – as also for many other examples – proved to be a reasonable choice not affecting the stiffness overly much. As seen in Figures 6(c) and 7 no hour-glassing occurs and the load-elongation curve is only slightly above the curve for Q1/d8v1 element. A similar result is obtained by Simo and Armero (1992) using the Q1/E4 element which did not show hour-glassing for this loading.

The above simulations of the time independent plastic limit case are carried out using the viscoplastic formulation with a small viscosity η. This small viscous effect is not visible in the final results presented here, however as is well known from the literature the computational performance of the global Newton-Raphson scheme is considerably improved. This is particularly helpful, as using the pure plastic formulation in combination with a pure displacement controlled loading it is hard to pass the limit point without convergence problems in the global solution scheme. Using the viscoplastic formulation with small viscosity instead almost no convergence problems with reasonable step-size are obtained. As mentioned in section 4 the special choice of the residual equation circumvents the ill-conditioning at small viscosities, an observation also reported for a similar algorithm in Runesson *et al.* (1999).

7.4 Elongation of a latex strip

This example is chosen to demonstrate the developed procedures for a structure with highly non-linear elastic and elasto-plastic material including a reversal of the loading. In Reese and Wriggers (1997) a three-term Ogden material (Ogden, 1972a) with compressible extension (Ogden, 1972b) and von Mises yield condition (von Mises, 1913) with non-linear isotropic plastic hardening law is used to describe the rate independent behavior of latex rubber. In our contribution the behavior of latex rubber is described by the functions (17), (18) and (19). The elastic material law becomes identical to the one used in Reese and Wriggers (1997), if $\Lambda \to \infty$ (Lamé-constant), $K \to \infty$, $\theta = 1$, $\Omega \to 1$ with $\Omega > 1$ are chosen (concerning the volumetric energy function, see Doll and Schweizerhof, 1997). The material constants are given in Table IV. The ratio $K/\mu > 10^4$ ensures nearly incompressible behavior already in the elastic region. The small value η for the viscosity implies time-independent plasticity.

The three-dimensional strip has the dimension $100 \times 100 \times 10$mm. Due to symmetry only one eighth has to be discretized with a regular mesh of $25 \times 4 \times 1$ solid elements, see Figure 8(a). Loading is applied by a given horizontal displacement u at the strip ends. First the maximum displacement $u = 150$mm (400 percent of initial length) is reached within 300 uniform steps. Then the initial displacement $u = 0$mm is recovered by reverse loading ("unloading") with 300 uniform steps. The vertical and normal displacements of the strip ends are always held fixed.

In Figure 9 the longitudinal force-elongation curves are plotted; the hysteresis effects as a consequence of the plastic deformation are obvious. The selectively reduced integrated Q1/d8v1 element yields the curve with the lowest values of the force. The mixed integrated Q1/d8v1-ζ element leads – as expected – to increasing loads with decreasing volumetric weight factor ζ

Constant	Value
μ_1 ($\equiv$ N/mm^2)	0.9394
α_1	1.3
μ_2 ($\equiv$ N/mm^2)	$-1.6 \cdot 10^{-3}$
α_2	-3.6
μ_3 ($\equiv$ N/mm^2)	$1.5 \cdot 10^{-4}$
α_3	7.46
K ($\equiv$ N/mm^2)	10^4
θ	1
Ω	1.001
τ_0 ($\equiv$ N/mm^2)	3.6
H ($\equiv$ N/mm^2)	75
H_2 ($\equiv$ N/mm^2)	$1.1 \cdot 10^5$
a	6.83
ω	1
η	10^{-4}

Table IV.
Material data for the latex strip

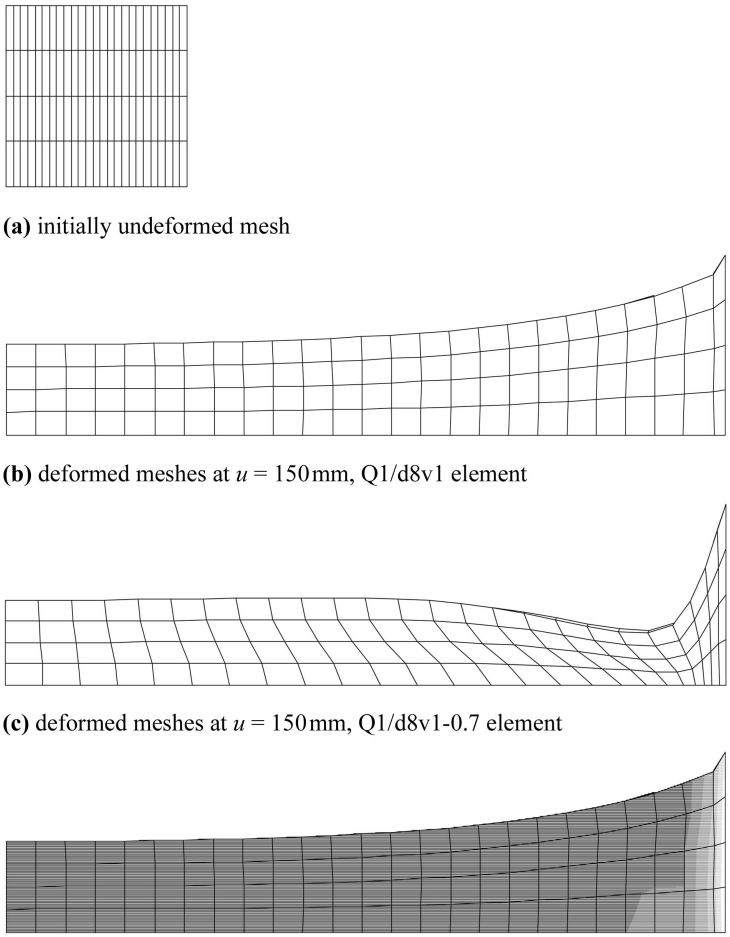

(a) initially undeformed mesh

(b) deformed meshes at u = 150 mm, Q1/d8v1 element

(c) deformed meshes at u = 150 mm, Q1/d8v1-0.7 element

(d) deformed meshes at u = 150 mm, equivalent plastic strain ξ (ξ_{min} = 0 and ξ_{max} = 0.073), Q1/d8v1 element

Figure 8.
Latex strip, eighth of strip

indicating the volumetric locking. Somewhere in the range of $\zeta < 0.7$ convergence of the global solution scheme is no longer achieved and the maximum displacement cannot be reached for the chosen step length due to the mentioned locking, which can also be observed from the result for the fully integrated Q1/d8v8 element, where no further deformation beyond 50mm was possible. As volumetric locking leads to larger loads, i.e. larger stresses which are only admitted for increased equivalent plastic strains ξ in the hardening part W^p in (17), the hysteresis effects are more pronounced for the elements with increased locking. The latter is visible for the hysteresis curve for $\zeta = 0.70$ in Figure 9. Due to plastic deformation the force becomes zero before the initial displacement $u = 0$mm is recovered for all $\zeta \geq 0.70$.

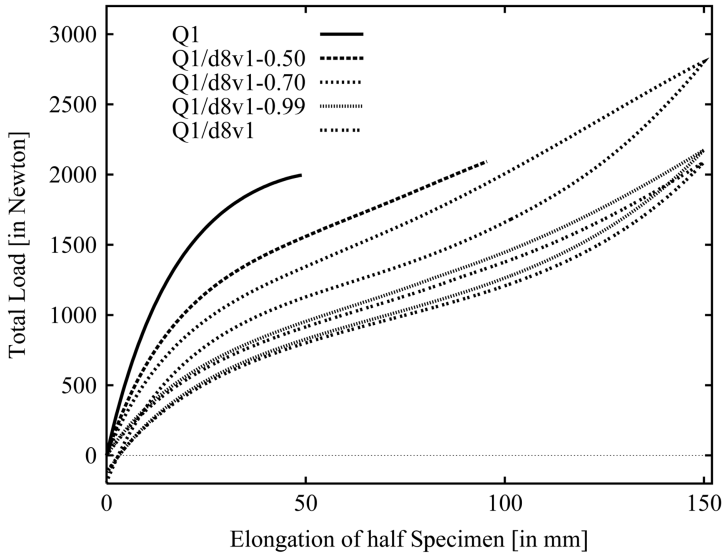

Figure 9.
Latex strip. Axial force versus elongation

Two representative meshes for the reduced integrated and mixed integrated elements at maximum elongation $u = 150$mm are depicted in Figure 8(b) and (c) to demonstrate the influence of slight volumetric locking on the behavior. As the vertical and normal displacements at the strip ends are held fixed, non-homogeneous deformations occur mainly in this area and the effect of the integration scheme for the volumetric terms is most important there. Due to volumetric locking the deformation of the Q1/d8v1-0.7 element is overconstrained and a non-physical deformation behavior near the strip ends is observed. In contrast, the Q1/d8v1 element leads to the expected physical result. Decreasing $\zeta < 0.7$ – thus increasing volumetric locking – the non-physical behavior increases until the global solution scheme diverges. Near the symmetry plane, where the deformation is nearly homogeneous, volumetric locking effects are less important. It should be noted, that due to the complete three-dimensional modeling and behavior of the strip with different thinning, the shown areas of the meshes in Figure 8(a)-(c) cannot be identical. In Figure 8(d) the equivalent plastic strain is plotted. Plastic deformations occur in the interior of the strip. At the strip ends the deformations remain elastic.

The Q1/d8v1 element exhibits mild hour-glassing at the strip ends, see Figure 8(b). Using a small stabilization instead with $\zeta = 0.99$ this effect vanishes completely without changing the load-elongation curve too much (see Figure 9). It is obvious, that for smaller ratios K/μ the results obtained with the Q1/d8v1-ζ element for various ζ-values would differ less from each other.

7.5 Bending of a thin square plate

This example is chosen to show the effect of the proposed algorithms on thin shell type structures at large deformations and is adopted from Büchter *et al.* (1994), Seifert (1996) and Miehe (1997). The square plate has a ratio thickness/

length t/l = 2.54/508 = 1/200. Due to the symmetry of the plate only a quarter is discretized with a uniform mesh of 9×9 shell elements, see Figure 10(a). A uniform reference load $p_0 = 3.94 \cdot 10^{-3}\text{N/mm}^3$ normal to the plate is applied. This specific volume-type loading is identical with an area load of 10^{-2}N/mm^3 divided by the plate thickness applied on the mid-plane. All edge displacements of the lower surface normal to the plate are held fixed while the in-plane displacements are free. Because the edge displacements of the upper surface are completely free, "edge-rotations" may occur.

The applied shell elements are so-called ANS3Dq resp. eas3Dq 8-node "solid-shell" elements which are three-dimensional continuum elements with specific enhancements to avoid locking in thin shell applications (for detaills, see Hauptmann, 1997; Hauptmann and Schweizerhof, 1998). The displacement interpolation is bilinear in in-plane direction and quadratic in normal shell direction. The ANS3Dq and the eas3Dq elements are formulated in the total material description using the 2. Piola-Kirchhoff stress tensor $\boldsymbol{S}$ and the Green-Lagrange strain tensor $\boldsymbol{E}$, i.e. the corresponding transformation has to be applied. According to Dvorkin and Bathe (1984) the assumed natural strain concept is employed for the transverse shear strains. Following the developments of Simo and others (Simo, 1992; Simo *et al.*, 1993) the in-plane membrane and bending strain terms are enhanced by a five-term incompatible strain function for the eas3Dq element. Because the deformation gradient is the driving variable for the algorithms presented in sections 3 and 4 a modified deformation gradient $\boldsymbol{F}_{mod}$ has to be computed from the assumed strain tensor $\boldsymbol{E}_{ANS}$ resp. in addition to the enhanced strain tensor $\boldsymbol{E}_{eas}$ for the eas3Dq element. Here $\boldsymbol{F}_{mod} = R \cdot \boldsymbol{U}_{mod}$ is composed of the unmodified rotation tensor $\boldsymbol{R} = \boldsymbol{F} \cdot \boldsymbol{U}^{-1}$ and the assumed right stretch tensor $\boldsymbol{U}_{mod} = (2\boldsymbol{E}_{mod} + 1)^{1/2}$.

The material behavior is described by the energy function (16), the yield condition (18) and the penalty function (19). In Table V the material data are

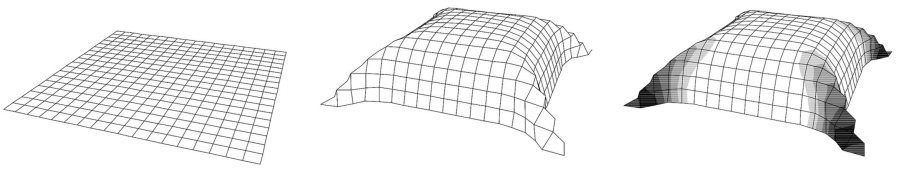

(a) initially undeformed plate

(b) deformed plate at load level $\lambda = 70.5$

(c) equivalent plastic strain ξ ($\xi_{min} = 0$ and $\xi_{max} = 0.166$) at load level $\lambda = 70.5$

Figure 10.
Thin square plate, ANS3Dq/d4v1 element

	Constant							
	μ ($\equiv$ N/mm^2)	K ($\equiv$ N/mm^2)	τ_0 ($\equiv$ N/mm^2)	H ($\equiv$ N/mm^2)	τ_∞ ($\equiv$ N/mm^2)	δ	ω	η
Value	26,538	57,500	248	0	248	10^{10}	1	0, 10^{-6}

Table V.
Material data for the thin square plate

given. The resulting isotropic material law is representing an elastic perfectly plastic behavior. The viscosity is assumed to be negligible and the results for $\eta = 0$ and $= 10^{-6}$ are compared. Both values for the viscosity η yield identical solutions and identical global convergence rates.

The ANS3Dq ($\equiv$ ANS3Dq/d4v4) resp. the eas3Dq elements are fully integrated with six Gauss-points in thickness direction and four Gauss-points in in-plane direction. The ANS3Dq/d4v1 resp. the eas3Dq elements employ full integration for the deviatoric part and reduced integration for the volumetric part, i.e. for the latter six Gauss-points in thickness direction and one center-point in in-plane direction. Loading is applied by arc-length control with a load factor λ that scales the reference load $p = \lambda p_0$. In Figure 11 the load-deflection curves are plotted. The ANS3Dq/d4v1 element leads to results very close to the results found in Büchter *et al.* (1994), Seifert (1996) and Miehe (1997). It is clearly visible, that the full integration with the ANS3Dq/d4v4 element exhibits volumetric locking. In the elastic region at small load factors the curves are nearly identical. As soon as plastic deformation is present, the stiffening behavior of the ANS3Dq/d4v4 element can be seen. The mesh of the deformed plate obtained with the ANS3Dq/d4v1 element is shown in Figure 10(b). In the plate corners large deformations occur. As depicted in Figure 10(c) these deformations are elastoplastic while the deformations in the center of the plate remain purely elastic. In this example no hour-glassing has been observed. The eas3Dq/d4v4 element leads to larger deformations when the locking of the ANS3Dq/d4v4 element is appearing, thus when the plastic behaviour is more dominant. However, it does not fully remove volumetric locking, as becomes visible when again selective reduced integration is applied, see the eas3dq/d4v1 element. This obvious difference which leads to fairly large differences in the displacements in this coarse mesh can be attributed to the non-linear effects which cannot be removed by the five-parameter in-plane enhancement of the strains.

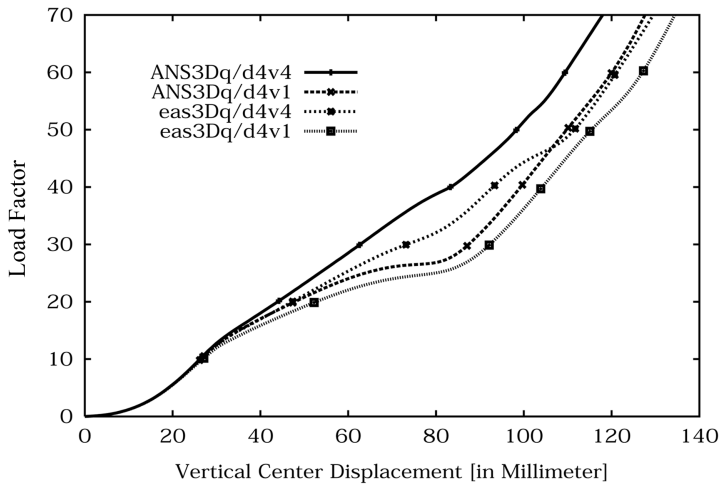

Figure 11.
Thin square plate. Load factor λ versus vertical center displacement

It is obvious that the used 9×9 mesh taken to compare with Büchter *et al.* (1994), Seifert (1996) and Miehe (1997), is by far not a converged mesh. Nevertheless, the locking effects are more visible in such coarse meshes. Further investigations of this example have been performed with refined meshes to obtain more accurate reference solutions (see, for example, Hauptmann and Schweizerhof, 1998; Harnau *et al.*, 2000).

8. Conclusions

If an isochoric-volumetric decoupled material behavior is assumed, the stress tensor and the consistent algorithmic moduli tensor can be additively decoupled into deviatoric and volumetric parts. For the general finite deformation case the splits of these tensors are derived for elasticity, plasticity and viscoplasticity in a spatial and in a total material description. Standard full integration leads to volumetric locking for isochoric deformations, in particular, in elements with non-rectangular shape. Using a one-point integration for the volumetric term, the well known selective reduced integration, the volumetric locking is completely removed, even for the elements with mixed hybrid formulation as the enhanced strain elements. All the selective reduced integrated elements do not show any kinematics resp. hour-glassing in the small deformation range, however under certain loading conditions and large deformations they exhibit hour-glassing similar as observed by Reese and Wriggers (1996), for the pure EAS-formulation. A simple but very efficient remedy is to introduce a mixed integration of the volumetric term by adding back a little of the stiffening fully integrated volumetric part by introducing the so-called Q1/d8v1-ζ element. Though a parameter must be chosen on experience, thus almost from heuristics only, the examples computed suggest that a small parameter is sufficient – an experience also expressed by Crisfield and Norris (1999).

To overcome the hour-glassing of the $\bar{\boldsymbol{F}}$ elements a modification similar to the mixed integration introduction of the volumetric term of the SRI elements is proposed.

The applicability of the SRI scheme to thin shell problems is also demonstrated using the solid-shell elements. In thickness direction an identical integration rule is chosen for the deviatoric and the volumetric terms. In in-plane direction selective reduced integration is employed for the volumetric term as for the solid elements improving the results considerably for the structural parts with isochoric deformation. For a more detailed discussion of the solid-shell elements with different interpolation and the removal of volumetric locking resp. the kinematics occurring at some loading state and their possible removal we refer to Harnau *et al.* (2000).

References

Büchter, N., Ramm, E. and Roehl, D. (1994), "Three-dimensional extension of non-linear shell formulation based on the enhanced assumed strain concept, *International Journal for Numerical Methods in Engineering*, Vol. 37, pp. 2551-68.

Chadwick, P. and Ogden, R.W. (1971), "A theorem of tensor calculus and its application to isotropic elasticity", *Archive for Rational Mechanics and Analysis*, Vol. 44, pp. 54-68.

Coleman, B.D. and Gurtin, M.E. (1967), "Thermodynamics with internal state variables", *Journal of Chemical Physics*, Vol. 47, pp. 597-613.

Coleman, B.D. and Noll, W. (1963), "The thermodynamics of elastic materials with heat conduction and viscosity", *Archive for Rational Mechanics and Analysis*, Vol. 13, pp. 167-78.

Crisfield, M.A. (1997), *Non-linear Finite Element Analysis of Solids and Structures. Volume 2: Advanced Topics*, John Wiley, Chichester.

Crisfield, M.A. and Norris, V. (1999), "A stabilized large-strain elasto-plastic Q1-P0 method", *International Journal for Numerical Methods in Engineering*, Vol. 46, pp. 579-92.

de Souza Neto, E.A., Perić, D., Dutko, M. and Owen, D.R.J. (1996), "Design of simple low order finite elements for large strain analysis of nearly incompressible solids", *International Journal of Solids and Structures*, Vol. 33, pp. 3277-96.

Doll, S. (1998), "Zur numerischen Behandlung grosser elasto-viskoplastischer Deformationen bei isochor-volumetrisch entkoppeltem Stoffverhalten", Report M98/2, Institut für Mechanik, Universität Karlsruhe.

Doll, S. and Schweizerhof, K. (1997), "On the development of volumetric strain energy functions", *Journal of Applied Mechanics*.

Dvorkin, E.N. and Bathe, K.J. (1984), "A continuum mechanics based four-node shell element for general non-linear analysis", *Engineering Computations*, Vol. 1, pp. 77-88.

Flory, P.J. (1961), "Thermodynamic relations for high elastic materials", *Transactions of the Faraday Society*, Vol. 57, pp. 829-38.

Fried, I. (1974), "Finite element analysis of incompressible material by residual energy balancing", *International Journal of Solids and Structures*, Vol. 10, pp. 993-1002.

Glaser, S. and Armero, F. (1997), "On the formulation of enhanced strain finite elements in finite deformations", *Engineering Computations*, Vol. 14, pp. 759-91.

Harnau, M., Hauptmann, R. and Schweizerhof, K. (2000), "Solid-shell elements with linear and quadratic shape functions at large deformations with nearly incompressible materials", forthcoming.

Hauptmann, R. (1997), "Strukturangepaßte geometrisch nichtlineare Finite Elemente für Flächentragwerke", Report M97/3, Institut für Mechanik, Universität Karlsruhe.

Hauptmann, R. and Schweizerhof, K. (1998), "A systematic development of 'solid-shell' element formulations for linear and non-linear analyses employing only displacement degrees of freedom", *International Journal for Numerical Methods in Engineering*, Vol. 42, pp. 49-69.

Hauptmann, R., Schweizerhof, K. and Doll, S. (1998), "Extension of the 'solid-shell' concept for application to large elastic and large elastoplastic deformations", *International Journal for Numerical Methods in Engineering*.

Hencky, H. (1933), "The elastic behavior of vulcanized rubber", *Journal of Applied Mechanics*, Vol. 1, pp. 45-53.

Hughes, T.J.R. (1977), "Equivalence of finite elements for nearly incompressible elasticity", *Journal of Applied Mechanics*, Vol. 44, pp. 181-3.

Hughes, T.J.R. (1980), "Generalization of selective integration procedures to anisotropic and non-linear media", *International Journal for Numerical Methods in Engineering*, Vol. 15, pp. 1413-18.

Hughes, T.J.R. (1987), *The Finite Element Method. Linear Static and Dynamic Finite Element Analysis*, Prentice-Hall, Englewood Cliffs, NJ.

Korelc, J. and Wriggers, P. (1996), "Consistent gradient formulation for a stable enhanced strain method for large deformations", *Engineering Computations*, Vol. 13, pp. 103-23.

Kröner, E. (1960), "Allgemeine Kontinuumstheorie der Versetzungen und Eigenspannungen", *Archive for Rational Mechanics and Analysis*, Vol. 4, pp. 273-334.

Lee, E.H. (1969), "Elastic-plastic deformation at finite strains", *Journal of Applied Mechanics*, Vol. 36, pp. 1-6.

Lee, E.H. and Liu, D.T. (1967), "Finite-strain elastic-plastic theory with application to plane-wave analysis", *Journal of Applied Physics*, Vol. 38, pp. 19-27.

Lemaitre, J. and Chaboche, J.-L. (1990), *Mechanics of Solid Materials*, Cambridge University Press, Boston, MA.

Liu, C.H., Hofstetter, G. and Mang, H.A. (1992), "Evaluation of 3D FE-formulations for incompressible hyperelastic materials at finite strains", in Hirsch, C., Zienkiewicz, O.C. and Oñate, E. (Eds), *Proceedings of the First European Conference on Numerical Methods in Engineering*, 7-11 September, Brussels, pp. 757-64.

Liu, C.H., Hofstetter, G. and Mang, H.A. (1994), "3D finite element analysis of rubber-like materials at finite strains", *Engineering Computations*, Vol. 11, pp. 111-28.

Luenberger, D.G. (1984), *Linear and Non-linear Programming*, Addison-Wesley, Reading, MA.

Malkus, D.S. (1976), "A finite element displacement model valid for any value of the compressibility", *International Journal of Solids and Structures*, Vol. 12, pp. 731-8.

Malkus, D.S. and Hughes, T.J.R (1978), "Mixed finite element methods – reduced and selective integration techniques: a unification of concepts", *Computer Methods in Applied Mechanics and Engineering*, Vol. 15, pp. 63-81.

Marsden, J. and Hughes, T.J.R (1983), *Mathematical Foundations of Elasticity*, Prentice-Hall, Englewood Cliffs, NJ.

Miehe, C. (1993), "Kanonische Modelle multiplikativer Elasto-Plastizität. Thermodynamische Formulierung und numerische Implementation", Report F93/1, Institut für Baumechanik und Numerische Mechanik, Universität Hannover.

Miehe, C. (1997), "A theoretical and computational model for isotropic elastoplastic stress analysis in shells at large strains", *Computer Methods in Applied Mechanics and Engineering*.

Moran, B., Ortiz, M. and Shih, C.F. (1990), "Formulation of implicit finite element methods for multiplicative finite deformation plasticity", *International Journal for Numerical Methods in Engineering*, Vol. 29, pp. 483-514.

Müller-Hoeppe, N. (1990), "Beiträge zur Theorie und Numerik finiter inelastischer Deformationen", Report F90/4, Institut für Baumechanik und Numerische Mechanik, Universität Hannover.

Nagtegaal, J.C. and Fox, D.D. (1996), "Using assumed enhanced strain elements for large compressive deformation", *International Journal of Solids and Structures*, Vol. 33, pp. 3151-9.

Nagtegaal, J.C., Parks, D.M. and Rice, J.R. (1974), "On numerically accurate finite element solutions in the fully plastic range", *Computer Methods in Applied Mechanics and Engineering*, Vol. 4, pp. 153-77.

Ogden, R.W. (1972a), "Large deformation isotropic elasticity – on the correlation of theory and experiment for incompressible rubberlike solids", *Proceedings of the Royal Society of London. Series A*, Vol. 326, pp. 565-84.

Ogden, R.W. (1972b), "Large deformation isotropic elasticity: on the correlation of theory and experiment for compressible rubberlike solids", *Proceedings of the Royal Society of London. Series A*, Vol. 328, pp. 567-83.

Ogden, R.W. (1984), *Non-linear Elastic Deformations*, Ellis Horwood, Chichester.

Perzyna, P. (1963), "The constitutive equations for rate sensitive plastic materials", *Quarterly of Applied Mathematics*, Vol. 20, pp. 321-32.

Perzyna, P. (1966), "Fundamental problems in viscoplasticity", *Advances in Applied Machanics*, Vol. 9, pp. 243-377.

Perzyna, P. (1971), "Thermodynamic theory of viscoplasticity", *Advances in Applied Mechanics*, Vol. 11, pp. 313-54.

Reese, S. (1994), "Theorie und Numerik des Stabilitätsverhaltens hyperelastischer Festkörper", doctoral thesis, Technische Hochschule Darmstadt.

Reese, S. and Wriggers, P. (1997), "A material model for rubber-like polymers exhibiting plastic deformation: computational aspects and a comparison with experimental results", *Computer Methods in Applied Mechanics and Engineering*, Vol. 148, pp. 279-98.

Reese, S. and Wriggers, P. (1999), "A stabilization technique to avoid hourglassing in finite elasticity", *International Journal for Numerical Methods in Engineering*.

Reese, S., Wriggers, P. and Reddy, D.D. (1999), "A new locking-free brick element technique for large deformation problems in elasticity", *Computers & Structures*.

Runesson, K., Ristinmaa, M. and Mähler, L. (1999), "A comparison of viscoplasticity formats and algorithms", *Mech. Cohes.-Frict. Mater.*, Vol. 4, pp. 75-98.

Schellekens, J.C.J and Parisch, H. (1994), "On finite deformation elasto-plasticity", ISD-Report 94/5, Institut für Statik und Dynamik der Luft- und Raumfahrtkonstruktionen, Universität Stuttgart.

Seifert, B. (1996), "Zur Theorie und Numerik finiter elastoplastischer Deformationen von Schalenstrukturen", Report F96/2, Institut für Baumechanik und Numerische Mechanik, Universität Hannover.

Simo, J.C. (1988), "A framework for finite strain elastoplasticity based on maximum plastic dissipation and the multiplicative decomposition: Part II. Computational aspects", *Computer Methods in Applied Mechanics and Engineering*, Vol. 68, pp. 1-31.

Simo, J.C. (1992), "Algorithms for static and dynamic multiplicative plasticity that preserve the classical return mapping schemes of the infinitesimal theory", *Computer Methods in Applied Mechanics and Engineering*, Vol. 99, pp. 61-112.

Simo, J.C. and Armero, F. (1992), "Geometrically non-linear enhanced strain mixed methods and the method of incompatible modes", *International Journal for Numerical Methods in Engineering*, Vol. 33, pp. 1413-49.

Simo, J.C. and Taylor, R.L. (1985), "Consistent tangent operators for rate-independent elastoplasticity", *Computer Methods in Applied Mechanics and Engineering*, Vol. 48, pp. 101-18.

Simo, J.C and Taylor, R.L. (1986), "A return mapping algorithm for plane stress elastoplasticity", *International Journal for Numerical Methods in Engineering*, Vol. 22, pp. 649-70.

Simo, J.C., Armero, F. and Taylor, R.L. (1993), "Improved versions of assumed enhanced strain tri-linear elements for 3D finite deformation problems", *Computer Methods in Applied Mechanics and Engineering*, Vol. 110, pp. 359-86.

Simo, J.C., Taylor, R.L. and Pister, K.S. (1985), "Variational and projection methods for volume constraint in finite deformation elasto-plasticity", *Computer Methods in Applied Mechanics and Engineering*, Vol. 51, pp. 177-208.

van den Bogert, P.A.J., de Borst, R., Luiten, G.T. and Zeilmaker, J. (1991), "Robust finite elements for 3D-analysis of rubber-like materials", *Engineering Computations*, Vol. 8, pp. 3-17.

von Mises, R. (1913), "Mechanik der festen Körper im plastisch-deformablen Zustand", Nachrichten von der Gesellschaft der Wissenschaten zu Göttingen, Mathematisch-Physikalische Klasse, pp. 582-92.

von Mises, R. (1928), "Mechanik der plastischen Formänderung von Kristallen", *Zeitschrift für angevandte Mathematik und Mechanikm*, Vol. 8, pp. 161-85.

Wriggers, P. and Reese, S. (1996), "A note on enhanced strain methods for large deformations", *Computer Methods in Applied Mechanics and Engineering*, Vol. 135, pp. 201-9.

Wriggers, P., Eberlein, R. and Reese, S. (1996), "A comparison of three-dimensional continuum and shell elements for finite plasticity", *International Journal of Solids and Structures*, Vol. 33, pp. 3309-26.